


Energetics of Microwaves Probed by Double Quantum Dot Absorption

Subhomoy Haldar^{1,*}, Harald Havir¹, Waqar Khan^{1,‡}, Sebastian Lehmann¹, Claes Thelander¹,
Kimberly A. Dick^{1,2} and Ville F. Maisi^{1,†}

¹NanoLund and Solid State Physics, Lund University, Box 118, 22100 Lund, Sweden

²Center for Analysis and Synthesis, Lund University, Box 124, 22100 Lund, Sweden

 (Received 3 August 2022; accepted 24 January 2023; published 23 February 2023)

We explore the energetics of microwaves interacting with a double quantum dot photodiode and show wave-particle aspects in photon-assisted tunneling. The experiments show that the single-photon energy sets the relevant absorption energy in a weak-drive limit, which contrasts the strong-drive limit where the wave amplitude determines the relevant-energy scale and opens up microwave-induced bias triangles. The threshold condition between these two regimes is set by the fine-structure constant of the system. The energetics are determined here with the detuning conditions of the double dot system and stopping-potential measurements that constitute a microwave version of the photoelectric effect.

DOI: [10.1103/PhysRevLett.130.087003](https://doi.org/10.1103/PhysRevLett.130.087003)

Microwaves have an important role in solid-state quantum systems in mediating interactions, control, and performing readout in quantum technology [1]. One particularly interesting subset of the field is semiconductor-superconductor hybrids where the microwave signals interact with low-dimensional semiconductors enabling coherent interactions together with electron transport [2]. One of the central nanostructures here is a double quantum dot (DQD) [3–5]. DQDs have been used for photon emission [6,7] up to masing regime [8–11], coherent interactions [12–15] including ultrastrong coupling limit [16], and microwave spectroscopy [17–19]. The recent theory by Wong and Vavilov [20], predicted, and the following experiment by Khan *et al.* [21] demonstrated that a cavity-coupled DQD yields an efficient photodiode in the microwave domain. Detection of microwave photons using DQDs is encouraging because of the capabilities offered due to the continuous mode of device operation with voltage-controlled energy levels [22–24]. However, most of these previous reports describing DQDs as microwave absorbers lack an explicit discussion of wave-particle interplay during the absorption process. It is often considered that the relevant threshold for the single-photon picture is when the resonator is loaded on average by one photon or less.

In this Letter, we, however, show that the single-photon absorption picture [3,4,21] sustains up to the cavity photon number $n_r^c = 9/16\alpha = 490$, set by the effective fine-structure constant $\alpha = (1/4)Z_0G_0$ with characteristic

impedance Z_0 of the resonator and conductance quantum G_0 . We probe the energetics [25,26] of the microwaves interacting with a DQD photodiode and determine the detuning conditions leading to photon-activated transport. These results are complemented with stopping-potential measurements that constitute a microwave version of the photoelectric effect showing the photoexcited electrons obtain nearly the full energy of the photons in the low-drive limit.

The hybrid device used in the experiments is realized by coupling a DQD system to a coplanar waveguide resonator, Fig. 1(a). Here, a crystal phase defined DQD is formed by two zinc blende islands separated by three wurtzite barriers in an InAs nanowire [21,27,28]. A GaSb shell, selectively grown on zinc blende segments and removed before making contacts, helps to locate the dots as seen in Fig. 1(b). Plunger gate voltages (V_{GL} , V_{GR}) control the electrochemical energies (E_L , E_R) of the respective dots. The drain contact couples directly to a coplanar resonator made of 100 nm thick Nb film. The resonator has a fundamental resonance at $f_r = 6.715$ GHz corresponding to photon energy $E_p = 27.7$ μ eV, and a loaded quality factor of $Q_L = 1320$ with lumped capacitance $C_r \approx 540$ fF and inductance $L_r \approx 1000$ pH. Details of our rf circuit and power calibration may be found in Ref. [21]. For standard transport, we apply a bias voltage V_b to the source and measure current I_{SD} from the voltage node point in the middle of the resonator. The nanowire also contains an additional dot (QD-3) for charge sensing, which is not used in this study. To avoid contribution from QD-3, we apply the same bias to the other side of QD-3, Fig. 1(a). Measurements are performed in a dilution fridge with a base temperature of 10 mK.

We first characterize the properties of the DQD by measuring a charge stability diagram without a microwave drive [Fig. 1(c)]. With $V_b = 1$ mV applied on the DQD,

Published by the American Physical Society under the terms of the [Creative Commons Attribution 4.0 International license](https://creativecommons.org/licenses/by/4.0/). Further distribution of this work must maintain attribution to the author(s) and the published article's title, journal citation, and DOI. Funded by [Bibsam](https://www.bibsam.se/).

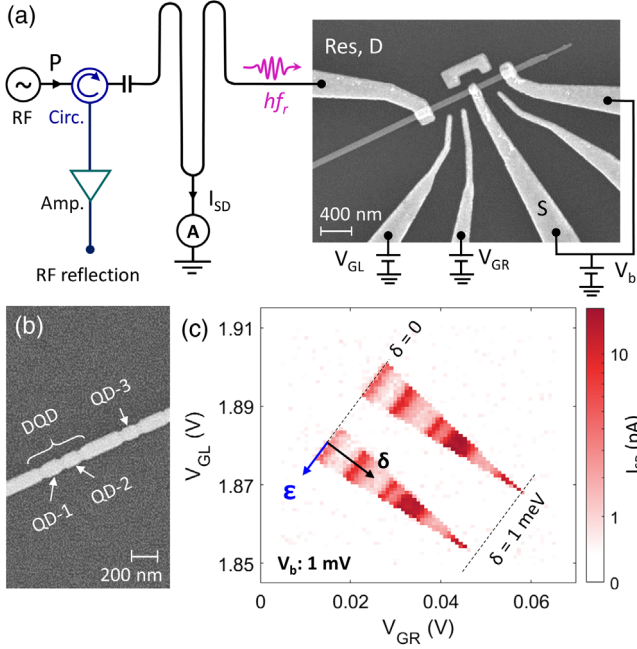


FIG. 1. (a) Scanning electron microscope image of the nanowire device and schematic diagram of the coplanar resonator and measurement setup. The central conducting line of the resonator connects the drain lead D of the DQD and allows us to measure I_{SD} via a voltage node point of the resonance mode. (b) The nanowire used for the device fabrication before removing the GaSb shell shows the individual dots. (c) Bias voltage V_b driven current I_{SD} as a function of V_{GL} and V_{GR} in the absence of a microwave drive.

sequential tunneling of electrons results in finite bias triangles (FBTs) at the charge triple points [4]. To specify the energy level positions, we define two local coordinates $\delta = (E_L - E_R)$ and $\epsilon = (E_L + E_R)/2$ representing difference and average energy of electronic states in the two dots [Fig. 1(c)]. Both δ and ϵ change linearly with the gate voltage, $\delta = \alpha_\delta^R \times \Delta V_{GR}$ and $\epsilon = \alpha_\epsilon^R \times \Delta V_{GR}$. This yields us the lever arms, $\alpha_\delta^R = 29.5$ and $\alpha_\epsilon^R = 75.3$ $\mu\text{eV}/\text{mV}$ along the two directions indicated in Fig. 1(c) with black and blue arrows, respectively [4,21]. From the charge stability diagram, we estimate the charging energies $E_{C,L} = 1.9$, $E_{C,R} = 2.2$ meV [28], and restrict our analysis to $\delta, \epsilon < E_C$ to allow only one excess electron in the DQD.

We now turn into the microwave response of the circuit. A continuous microwave tone is sent into the resonator via a capacitively coupled input port, Fig. 1(a). The DQD resides at the voltage antinode on the other end of the $\lambda/2$ resonator. The electrical dipole moments of the DQD charge states hence interact with voltage oscillations at the end of the resonator [12]. Figures 2(a)–2(c) present the measured I_{SD} through the DQD at power $P = 1, 100, \text{ and } 10\,000$ fW, respectively. Panel (a) with the lowest power shows finite I_{SD} at two points with polarity reversal. These points correspond to the cases where the energy

difference of the bonding and antibonding states of the DQD, given by $E = \sqrt{\delta^2 + (2t)^2}$, matches the single-photon energy E_p , which corresponds to the “microwave as a particle” scenario [21]. The energy diagrams in the insets illustrate this with vanishing hybridization. With larger microwave power, panels (b) and (c), the two points increase in size and eventually form microwave induced triangles (MWTs) with the same shape as the FBTs of Fig. 1(c). Interestingly, in contrast to the low-power limit, the active regions extend now both in the positive and negative δ directions. The formation of these MWTs in electronic transport was not presented in the earlier reports even under high microwave power [4,18,29,30]. The faint photo-current signal outside the MWTs of Fig. 2(c) arises most likely due to the charge cotunneling across the transparent QD-lead barrier of the DQD [4].

To understand the energy scales governing the formation of the MWTs, we repeat in Fig. 2(d) a microwaves-driven stability diagram for a high-power case schematically together with the key detuning points for our analysis marked with A, B, C, and C'. We begin by identifying the $(\delta, \epsilon) = (0, 0)$ point marked in blue based on the symmetries of the two overlapping MWTs. Along the $\delta = 0$ line, we obtain a finite I_{SD} up to the points where the energy ϵ_{max} of adding an electron into the DQD, point C, or the energy of removing an electron from the dot $-\epsilon_{\text{max}}$, point C', exceeds what is available from the microwave-drive. Figure 2(e) presents the corresponding energy band diagrams. The data of Fig. 2(c) yields the value $\epsilon_{\text{max}} = 520$ μeV for $P = 10$ pW. In a steady state, photocurrent depends on the fraction of time when the DQD energy levels (E_L, E_R) remain below the Fermi energy of the drain. Thus, the approximately sinusoidal behavior of I_{SD} , as seen in the inset of Fig. 2(c), represents the microwave waveform interacting with the Fermi energy of the drain.

Moving from point C of Fig. 2(d) towards either A or B along the edge of the red MWT keeps the energy level E_L fixed while changing E_R . Moving from C towards A introduces an energy cost $-\delta$ needed for the interdot transition from left QD to the right one reaching its maximum $-\delta = \delta_A$ at point A as presented in Fig. 2(f). From Fig. 2(c), we determine $\delta_A = 370$ μeV as the largest amount of energy provided by the microwave drive with $P = 10$ pW.

When moving from point C instead to point B, energy is gained in the interdot transition. Here, in addition to photons, phonons play a major role in absorbing the energy [6,7]. Interestingly the maximum energy $\delta = \delta_B = 880$ μeV at point B as shown in panels (c) and (g) is larger than ϵ_{max} . This implies that the electron enters the S reservoir at an energy $\delta_B - \epsilon_{\text{max}} = 360$ μeV below the Fermi energy, see Fig. 2(g). This is possible only if part of the microwave drive appears across the right QD-S barrier. A simple estimate that the rf-amplitude V_{MW} is divided roughly equally over the three junction capacitances is

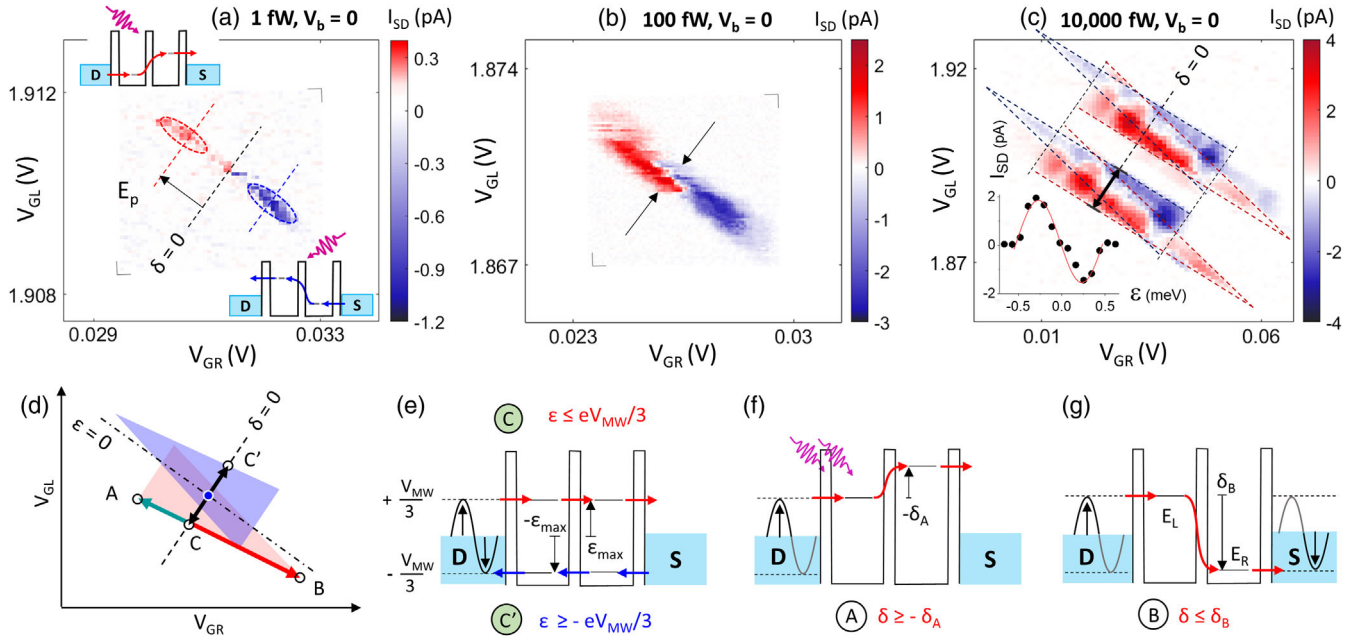


FIG. 2. (a)–(c) Photocurrent as a function of V_{GR} and V_{GL} with $V_b = 0$ and $P = 1$ (a), 100 (b), and 10 000 fW (c). Inset of (c) shows I_{SD} as a function of ε at $\delta = 0$. Dashed lines drawn in panels (a) and (c) are guides for the eye. (d) Schematic diagram of the overlapping microwave-induced triangles with the critical points A, B, C, and C' for the analysis. The triangles extend both in the positive and negative detuning δ directions along with a finite spread in the ε axis (line CC' for the $\delta = 0$ case). (e)–(g) Energy band diagrams and threshold conditions for points C and C' (e), point A with negative detuning $\delta = -\delta_A$ (f), and point B with positive detuning $\delta = \delta_B$ (g). The sinusoidal curves of figures (e)–(g) indicate the effective microwave amplitude $V_{MW}/3$ across each junction resulting from a capacitive division of V_{MW} evenly over the three junctions: The chemical potential of the drain oscillates with full voltage amplitude V_{MW} , whereas the source is grounded. With the voltage division set by equal junction capacitances, the energy level of the left dot oscillates then with $2V_{MW}/3$, and the right one with $V_{MW}/3$, leading to the effective amplitude of $V_{MW}/3$ in each junction.

supported by the finding that the corresponding energy costs, ε_{max} , δ_A , and $(\delta_B - \varepsilon_{max})$ are approximately equal.

Figure 3 presents δ_A , δ_B , and ε_{max} as a function of P . As seen in Fig. 3, both δ_A and δ_B as well as ε_{max} all increase proportional to $P^{1/2}$ over 2 orders of magnitude in the power. This indicates the amplitude $V_{MW} \propto P^{1/2}$ sets the relevant energy for the transport. To estimate V_{MW} across the DQD, we use the result of Ref. [31], which considers the standing wave in the resonator by circulating the input power for Q_L oscillation periods and hence increasing the amplitude to

$$V_{MW} = \left(\frac{4Q_L^2 Z_0}{Q_{ex}} \times P \right)^{1/2}. \quad (1)$$

Here, $Z_0 \approx 60 \Omega$ is the resonator impedance, and $Q_{ex} = 1820$ is the external quality factor. As shown by the solid lines of Fig. 3, one-third of the estimated microwave-amplitude per junction, $eV_{MW}/3$, catches well the relevant energy costs in the large P region. Correspondingly the number of photons stored in the resonator is obtained as the ratio of energy stored in the resonator to the photon energy, $n_r = \frac{1}{2} C_r V_{MW}^2 / E_P$, which we depict in Fig. 3.

For $P < 100$ fW, the interdot absorption energy δ_A saturates to E_P [Fig. 3(a)]. This is the smallest energy

quanta that can be absorbed from the microwave drive. The saturation takes place at $eV_{MW}/3 \lesssim E_P$ when the energy related to the amplitude is not sufficient to provide energy greater than the photon energy. For δ_B and ε_{max} , the saturation is not present. These two energies are related to the tunneling between one of the discrete QD energy levels and the continuum of states in either source or drain in contrast to tunneling between the discrete energy levels in the interdot process.

The threshold condition, $eV_{MW}/3 = E_P$, yields the corresponding cavity photon number $n_r^c = \frac{1}{2} C_r (3E_P/e)^2 / E_P = 9/16\alpha$, where $\alpha = (1/4)Z_0 G_0$ is the fine-structure constant of the system. The blue dashed line of Fig. 3(a) marks the threshold value $n_r^c = 490$, which is in good agreement with the threshold in our experiment. Thus, the single-photon picture holds up to the large photon number of $n_r^c = 490$ set by the resonator impedance level via α together with the prefactor of $(m/4)^2$, where $m = 3$ arises from the number of junctions over which the resonator voltage is divided.

An alternative approach to determine the absorption energetics is to apply a bias V_b to stop the photocurrent. This is analogous to the famous photoelectric effect of optical photons. In Figs. 4(a)–4(e), we show the effect of V_b on the photoresponse. The middle panel repeats the

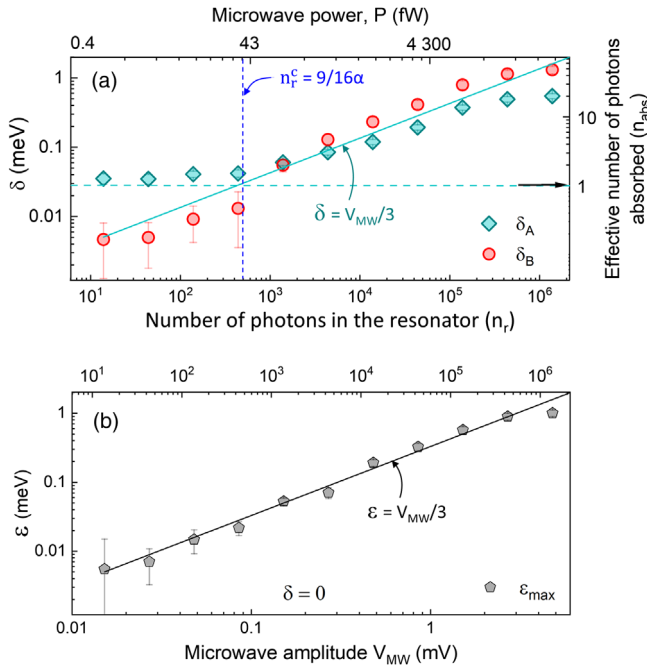


FIG. 3. (a): Detuning δ_A and δ_B as a function of microwave power P . Here, the solid green line corresponds to $\delta = V_{MW}/3$ and the dashed line $\delta = E_P$. The corresponding number of photons ($n_{\text{abs}} = \delta_A/E_P$) contributing to an absorption event is also shown on the right-hand side. (b): Energy ϵ_{max} of the MWTs as a function of P . The microwave amplitude V_{MW} corresponding to the input powers are also indicated.

results at no applied bias. Once we apply a positive V_b , the negative MWT starts to shrink and finally vanishes as seen in Figs. 4(d) and 4(e). Similarly, the positive MWT diminishes for $V_b < 0$ as presented in 4(a) and 4(b). Figures 4(f)–4(h) show the maximum values of positive and negative current as a function of V_b for three microwave powers. The stopping-potential V_b^s marked with black arrows is the point where the reverse direction current $I_{SD} < 0$ vanishes.

At the low-drive limit of Fig. 4(f), we have $eV_b^s \approx E_P$. The amplitude V_{MW} is low and hence the energy gain of the transported electrons is set by E_P of the interdot process as depicted in the inset. For the higher power of Figs. 4(g) and 4(h), stopping-potential increases and follows $V_b^s \propto P^{1/2}$, which again reflects that the amplitude rather than the photon energy sets the relevant energy scale. For $P = 100$ and 10000 fW, we have $V_b^s = V_{MW}/3$, i.e., the energy gained out of only one of the three tunneling processes. We interpret this to arise from the opposite direction current dominating the transport before reaching $V_b^s = eV_{MW}$, where energy would be gained in all of the three tunneling events. As depicted in the inset of Fig. 4(h), the threshold for the competing opposite current is at $V_b^s = V_{MW}/3$ when the amplitude across the right quantum dot and source overcomes the energy cost for tunneling into the DQD as indicated with the blue arrow.

In conclusion, we studied the energetics of a microwave signal absorbed by a DQD photodiode and explored the

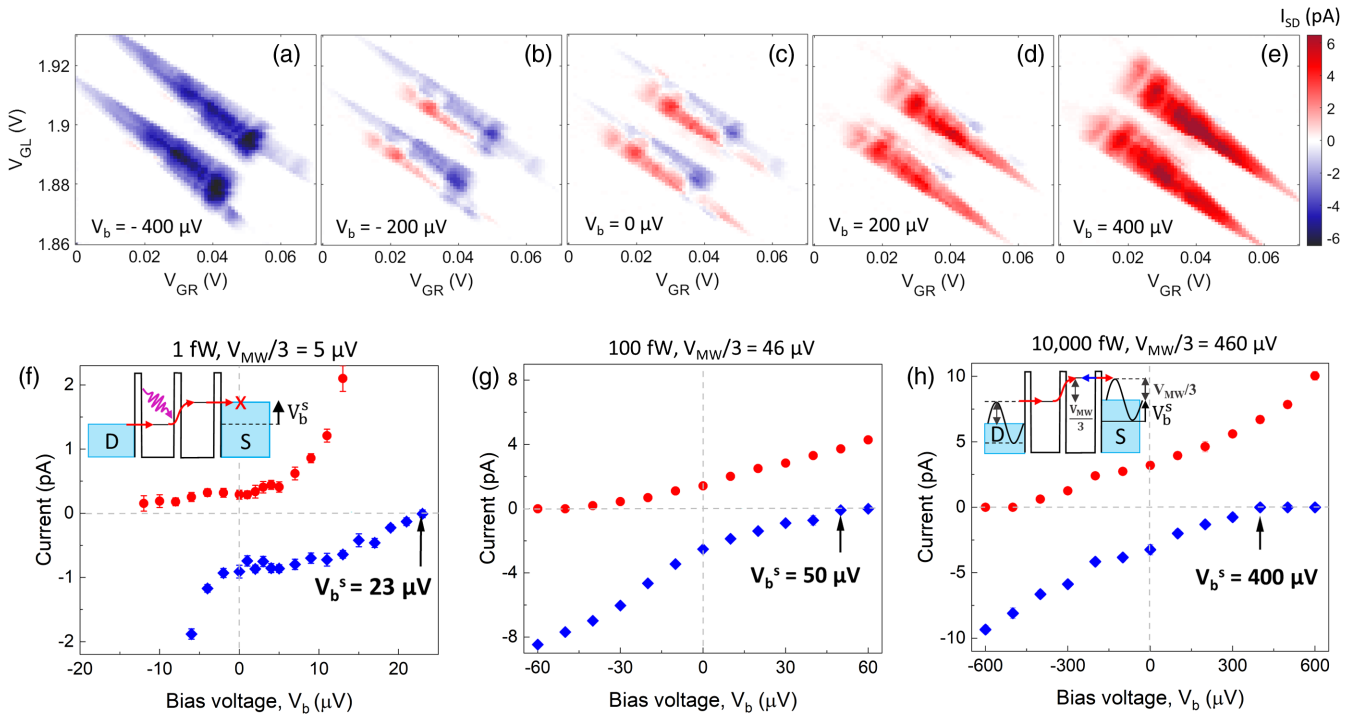


FIG. 4. (a)–(e): Photocurrent I_{SD} as a function of the plunger gate voltages for $P = 10$ pW and applied bias voltage V_b ranging from -400 to 400 μV . (f)–(h): Positive (red) and negative (blue) I_{SD} as a function of V_b for $P = 1, 100, 10\,000$ fW, respectively.

wave-particle interplay during the absorption process. At the threshold condition, the number of photons stored in the resonator is solely determined by the fine-structure constant of the system. We demonstrated that the single-photon absorption picture sustains up to hundreds of photons stored in the resonator. These findings also predict that for the high-impedance resonators with $Z_0 \sim 1/G_0$ [3,14], the fine-structure constant approaches unity, and $n_c^* \sim 1$, so that the system switches from the single-photon “particle” picture to the voltage-amplitude dominated regime immediately when the first photon is loaded into the cavity. Our results demonstrate a microwave version of the famous photoelectric effect and set an important milestone in bringing this key quantum optics concept to the experimental realm in the microwave domain. The present work opens up avenues of experiments using electron energy gain or loss spectroscopy in the microwave regime and shows the possibility of using a cavity-coupled DQD as the microwave energy harvester.

We acknowledge fruitful discussions with Adam Burke, Sven Dorsch, Martin Leijnse, Andreas Wacker, and Peter Samuelsson and the financial support from NanoLund, Swedish Research Council (Dnr 2019-04111), the Foundational Questions Institute, a donor advised fund of Silicon Valley Community Foundation (FQXi-IAF19-07), and the Knut and Alice Wallenberg Foundation through the Wallenberg Center for Quantum Technology (WACQT).

*subhomoy.haldar@ftf.lth.se

†ville.maisi@ftf.lth.se

‡Present address: VTT Technical Research Centre of Finland, Box 1000, 02044, Finland.

- [1] X. Gu, A. F. Kockum, A. Miranowicz, Y. Liu, and F. Nori, Microwave photonics with superconducting quantum circuits, *Phys. Rep.* **718–719**, 1 (2017).
- [2] G. Burkard, M. J. Gullans, X. Mi, and J. R. Petta, Superconductor–semiconductor hybrid-circuit quantum electrodynamics, *Nat. Rev. Phys.* **2**, 129 (2020).
- [3] L. Childress, A. S. Sørensen, and M. D. Lukin, Mesoscopic cavity quantum electrodynamics with quantum dots, *Phys. Rev. A* **69**, 042302 (2004).
- [4] W. G. van der Wiel, S. De Franceschi, J. M. Elzerman, T. Fujisawa, S. Tarucha, and L. P. Kouwenhoven, Electron transport through double quantum dots, *Rev. Mod. Phys.* **75**, 1 (2002).
- [5] A. Chatterjee, P. Stevenson, S. De Franceschi, A. Morello, N. P. de Leon, and F. Kuemmeth, Semiconductor qubits in practice, *Nat. Rev. Phys.* **3**, 157 (2021).
- [6] Y.-Y. Liu, K. D. Petersson, J. Stehlik, J. M. Taylor, and J. R. Petta, Photon Emission from a Cavity-Coupled Double Quantum Dot, *Phys. Rev. Lett.* **113**, 036801 (2014).
- [7] A. Stockklauser, V. F. Maisi, J. Basset, K. Cujia, C. Reichl, W. Wegscheider, T. Ihn, A. Wallraff, and K. Ensslin, Microwave Emission from Hybridized States in a Semiconductor Charge Qubit, *Phys. Rev. Lett.* **115**, 046802 (2015).
- [8] P.-Q. Jin, M. Marthaler, J. H. Cole, A. Shnirman, and G. Schön, Lasing and transport in a quantum-dot resonator circuit, *Phys. Rev. B* **84**, 035322 (2011).
- [9] Y.-Y. Liu, J. Stehlik, C. Eichler, M. Gullans, J. M. Taylor, and J. R. Petta, Semiconductor double quantum dot micromaser, *Science* **347**, 285 (2015).
- [10] M. J. Gullans, Y.-Y. Liu, J. Stehlik, J. R. Petta, and J. M. Taylor, Phonon-Assisted Gain in a Semiconductor Double Quantum Dot Maser, *Phys. Rev. Lett.* **114**, 196802 (2015).
- [11] B. K. Agarwalla, M. Kulkarni, and D. Segal, Photon statistics of a double quantum dot micromaser: Quantum treatment, *Phys. Rev. B* **100**, 035412 (2019).
- [12] T. Frey, P. J. Leek, M. Beck, A. Blais, T. Ihn, K. Ensslin, and A. Wallraff, Dipole Coupling of a Double Quantum Dot to a Microwave Resonator, *Phys. Rev. Lett.* **108**, 046807 (2012).
- [13] X. Mi, J. Cady, D. Zajac, P. Deelman, and J. R. Petta, Strong coupling of a single electron in silicon to a microwave photon, *Science* **355**, 156 (2017).
- [14] A. Stockklauser, P. Scarlino, J. V. Koski, S. Gasparinetti, C. K. Andersen, C. Reichl, W. Wegscheider, T. Ihn, K. Ensslin, and A. Wallraff, Strong Coupling Cavity QED with Gate-Defined Double Quantum Dots Enabled by a High Impedance Resonator, *Phys. Rev. X* **7**, 011030 (2017).
- [15] N. Samkharadze, G. Zheng, N. Kalhor, D. Brousse, A. Sammak, U. Mendes, A. Blais, G. Scappucci, and L. Vandersypen, Strong spin-photon coupling in silicon, *Science* **359**, 1123 (2018).
- [16] P. Scarlino, J. H. Ungerer, D. J. van Woerkom, M. Mancini, P. Stano, C. Muller, A. J. Landig, J. V. Koski, C. Reichl, W. Wegscheider, T. Ihn, K. Ensslin, and A. Wallraff, In-Situ Tuning of the Electric Dipole Strength of a Double Dot Charge Qubit: Charge Noise Protection and Ultra Strong Coupling, *Phys. Rev. X* **12**, 031004 (2022).
- [17] C. A. Stafford and N. S. Wingreen, Resonant Photon-Assisted Tunneling Through a Double Quantum Dot: An Electron Pump from Spatial Rabi Oscillations, *Phys. Rev. Lett.* **76**, 1916 (1996).
- [18] T. Oosterkamp, T. Fujisawa, W. Van Der Wiel, K. Ishibashi, R. Hijman, S. Tarucha, and L. P. Kouwenhoven, Microwave spectroscopy of a quantum-dot molecule, *Nature (London)* **395**, 873 (1998).
- [19] D. M. T. van Zanten, D. Sabonis, J. Suter, J. I. Väyrynen, T. Karzig, D. I. Pikulin, E. C. T. O’Farrell, D. Razmadze, K. D. Petersson, P. Krogstrup, and C. M. Marcus, Photon-assisted tunnelling of zero modes in a majorana wire, *Nat. Phys.* **16**, 663 (2020).
- [20] C. H. Wong and M. G. Vavilov, Quantum efficiency of a single microwave photon detector based on a semiconductor double quantum dot, *Phys. Rev. A* **95**, 012325 (2017).
- [21] W. Khan, P. P. Potts, S. Lehmann, C. Thelander, K. A. Dick, P. Samuelsson, and V. F. Maisi, Efficient and continuous microwave photoconversion in hybrid cavity-semiconductor nanowire double quantum dot diodes, *Nat. Commun.* **12**, 5130 (2021).
- [22] A. Ghirri, S. Cornia, and M. Affronte, Microwave photon detectors based on semiconducting double quantum dots, *Sensors* **20**, 4010 (2020).
- [23] S. Gustavsson, M. Studer, R. Leturcq, T. Ihn, K. Ensslin, D. C. Driscoll, and A. C. Gossard, Frequency-Selective

- Single-Photon Detection Using a Double Quantum Dot, *Phys. Rev. Lett.* **99**, 206804 (2007).
- [24] D. Zenelaj, P. P. Potts, and P. Samuelsson, Full counting statistics of the photocurrent through a double quantum dot embedded in a driven microwave resonator, *Phys. Rev. B* **106**, 205135 (2022).
- [25] C. Bergenfeldt, P. Samuelsson, B. Sothmann, C. Flindt, and M. Büttiker, Hybrid Microwave-Cavity Heat Engine, *Phys. Rev. Lett.* **112**, 076803 (2014).
- [26] J. J. Viennot, M. R. Delbecq, M. C. Dartiailh, A. Cottet, and T. Kontos, Out-of-equilibrium charge dynamics in a hybrid circuit quantum electrodynamics architecture, *Phys. Rev. B* **89**, 165404 (2014).
- [27] L. Namazi, M. Nilsson, S. Lehmann, C. Thelander, and K. A. Dick, Selective gasb radial growth on crystal phase engineered inas nanowires, *Nanoscale* **7**, 10472 (2015).
- [28] D. Barker, S. Lehmann, L. Namazi, M. Nilsson, C. Thelander, K. A. Dick, and V. F. Maisi, Individually addressable double quantum dots formed with nanowire polytypes and identified by epitaxial markers, *Appl. Phys. Lett.* **114**, 183502 (2019).
- [29] A. Wacker, A.-P. Jauho, S. Zeuner, and S. J. Allen, Sequential tunneling in doped superlattices: Fingerprints of impurity bands and photon-assisted tunneling, *Phys. Rev. B* **56**, 13268 (1997).
- [30] P. Tien and J. Gordon, Multiphoton process observed in the interaction of microwave fields with the tunneling between superconductor films, *Phys. Rev.* **129**, 647 (1963).
- [31] J. M. Sage, V. Bolkhovsky, W. D. Oliver, B. Turek, and P. B. Welander, Study of loss in superconducting coplanar waveguide resonators, *J. Appl. Phys.* **109**, 063915 (2011).